ACS Catalysis

Research Article

pubs.acs.org/acscatalysis

Pt-Poisoning-Free Efficient CO Oxidation on Pt_3Co Supported on MgO(100): An Ab Initio Study

Rafia Ahmad and Abhishek K. Singh*

Materials Research Centre, Indian Institute of Science, Bangalore 560012, India

Supporting Information

ABSTRACT: Late-transition-metal-doped Pt clusters are prevalent in CO oxidation catalysis, as they exhibit better catalytic activity than pure Pt, while reducing the effective cost and poisoning. However, completely eliminating the critical problem of Pt poisoning still poses a big challenge. Here, we report for the first time that, among the bimetallic clusters ((Pt_3M where M = Co, Ni, and Cu)/MgO(100)), the CO adsorption site inverts for Pt_3Co/MgO(100) from Pt to Co, due to the complete uptake of Pt d-states by lattice oxygen. While this resolves the problem of Pt poisoning, good reaction kinetics are predicted through low barriers for Langmuir–Hinshelwood and Mars van Krevelen (MvK) mechanisms of CO oxidation for Pt_3Co/MgO(100) and Li-doped MgO(100), respectively. Li doping in MgO(100) compensates for the charge imbalance caused by a spontaneous oxygen vacancy formation. Pt_3Co/Li-doped MgO(100) stands out as an exceptional CO oxidation catalyst, giving an MvK reaction barrier as low as 0.11 eV. We thereby propose a novel design strategy of d-band center inversion for CO oxidation catalysts with no Pt poisoning and excellent reaction kinetics.

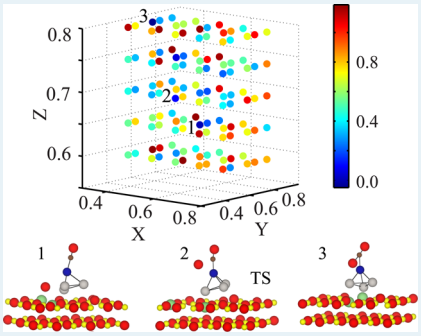

KEYWORDS: *bimetallic clusters, CO oxidation, catalysis, Pt poisoning free, density functional theory*

INTRODUCTION

CO oxidation to CO_2 is vital in automotive exhausts and low-temperature fuel cells for environmental and health-friendly emissions.[1,2] Noble metals such as gold,[3−6] platinum,[7−10] and palladium[11,12] have been extensively studied and practically used as oxygen reduction and CO oxidation catalysts. Platinum among these has shown the most remarkable catalytic efficiency in fuel cell cathode materials,[13] water−gas shift, hydrogenation,[14] oxygen reduction reactions (ORR),[15,16] and oxidation reactions including CO oxidation,[17,18] becoming an irreplaceable constituent for the same. Platinum nanoclusters have become a fundamental topic of investigation for CO oxidation pertaining to their high catalytic surface area and the molecular level insights they provide for reactions on metal surfaces.[19,20] Challenges associated with Pt-based catalysts are the high cost, low abundance, and rapid deactivation of the catalyst by CO poisoning. This to a certain extent can be overcome by replacing platinum with transition/secondary metals, which retain/improve the high catalytic nature of the parent cluster.[21−24] Alloying the platinum cluster with Ni, Cu, Co, and other transition metals manipulates the geometrical and electronic structure[25] of the resulting cluster, in particular, the d-states, to give the enhanced catalytic properties.[9,26,27]

Although various studies[28,29] have shown Pt bimetallic systems to exhibit better catalytic activities and lower CO poisoning effect, complete elimination of Pt poisoning is still unresolved. Here, we report the effect of late transition metal (Co, Ni, and Cu) doping in the pure Pt_4 cluster for CO oxidation and explore the mechanism of CO oxidation catalytic activity at an atomistic level. We report for the first time that, for Pt_3Co/MgO(100), the preferred CO adsorption site inverts to Co from Pt. This inversion results from the better availability of empty antibonding d-states of the Co atom in Pt_3Co than those of the Pt atoms. This can effectively address the issue of Pt degradation by CO. Furthermore, we predict the CO oxidation reaction kinetics by calculating the minimum energy pathway and the reaction barrier. Low CO oxidation reaction barriers by the Langmuir–Hinshelwood (L–H) mechanism on free-standing and supported Pt_3Co clusters indicate good catalytic activity. Even for the Mars van Krevelen (MvK) mechanism of CO oxidation on Pt_3Co/Li-doped MgO(100), a low reaction barrier of 0.11 eV predicts good reaction kinetics. Li-doped MgO(100) has a spontaneous activation of oxygen vacancy on attaching to the Pt_3Co cluster, while Li atoms maintain the charge balance. The present work exhibits the efficiency of the Pt_3Co/MgO(100) cluster in terms of no Pt poisoning and good reaction kinetics.

METHODS

The first-principles calculations were performed using density functional theory as implemented in the Vienna Ab Initio Simulation package. Electron–ion interactions were described using all-electron projector-augmented wave pseudopotentials. Electronic exchange and correlation were approximated by a Perdew–Burke–Ernzerhof generalized gradient approximation. The periodic images are separated by a 15 Å vacuum along

Received: December 1, 2014
Revised: February 3, 2015
Published: February 11, 2015

DOI: 10.1021/cs501911r
ACS Catal. 2015, 5, 1826−1832

three directions. For all of the free-standing cluster calculations, the Brillouin zone is sampled by a Γ point. For the clusters supported on substrate systems, a well-converged *k*-mesh of 7 × 7 × 1 was employed. A conjugate gradient scheme is used to relax the structures until the component of the forces on each atom was <0.005 eV Å $^{-1}$. The cutoff energy was set to 400 eV to ensure the accuracy of the results. The minimization of the reaction pathways and the search of the transition states (TS) have been performed with the steepest-descent nudged elastic band (NEB) method.[30,31] The CO oxidation reaction pathway and barrier were then calculated by NEB method through the identified TS.

RESULTS AND DISCUSSION

In order to gain insight into the effects of the substrate on the catalytic efficiency of the Pt/bimetallic clusters (Pt_4 and Pt_3M (M = Co, Ni, and Cu)), we begin our study with a complete analysis of CO oxidation on free-standing clusters. The tetrahedral geometry has been reported as the lowest energy structure of Pt_4;[32] these small Pt clusters have been reported as CO oxidation catalysts in a molecular beam experiment.[33] Platinum tetramers are frequently studied both experimentally[34,35] and theoretically[36] to gain insights in various catalytic mechanisms. The tetrahedral geometry of Pt_4 is shown in Supporting Information Figure S1. In this Pt_4 cluster, one of the atoms is replaced with Co, Ni, and Cu to obtain stable and relaxed geometries of Pt_3Co, Pt_3Ni, and Pt_3Cu, as shown in Figure 1a. The bond length between Pt and the included

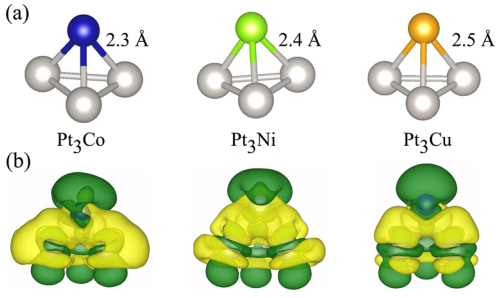

Figure 1. (a) Relaxed geometries of Pt_3Co, Pt_3Ni, and Pt_3Cu. (b) Charge redistribution plots of Pt_3Co, Pt_3Ni, and Pt_3Cu. Yellow and green represent the charge accumulation and depletion, respectively. Silver, blue, green, and gold represent Pt, Co, Ni, and Cu atoms, respectively.

transition metal (M) increases from left to right of the periodic table as 2.3, 2.4, and 2.5 Å for Pt−Co, Pt−Ni, and Pt−Cu, respectively. These bond lengths are reduced compared to 2.7 Å for Pt−Pt in the pure platinum cluster.

The bond length trend is understood from the amount of charge transfer from Pt to the transition metals, which can be visualized from charge redistribution, calculated as

$$\Delta\rho = \rho(Pt_3M) - \rho(Pt_3) - \rho(M)$$

where $\rho(Pt_3M)$, $\rho(Pt_3)$, and $\rho(M)$ are the charge densities of isolated systems of Pt_3M, Pt_3, and M, respectively. These charge accumulation and depletion plots are shown in Figure 1b. The Pt_3Co cluster shows the maximum redistribution, indicating the largest charge transfer from Pt, hence having the smallest bond length. The bond length increases with increasing number of d-electrons in the transition metal (Pt−Co < Pt−Ni < Pt−Cu), which is also the reason for the observed charge redistribution behavior in Figure 1b. This is further confirmed by conducting the Bader analysis[37,38] for the studied clusters. The Bader charge transfer from Pt atoms to M in Pt_3Co, Pt_3Ni, and Pt_3Cu are 1.1*e*, 0.6*e*, and 0.4*e*, respectively, following the trend of increasing bond length.

Next, CO adsorption was done on each cluster followed by a complete geometrical relaxation. The fully relaxed systems of CO-adsorbed clusters are shown in the insets of Figure 2. CO

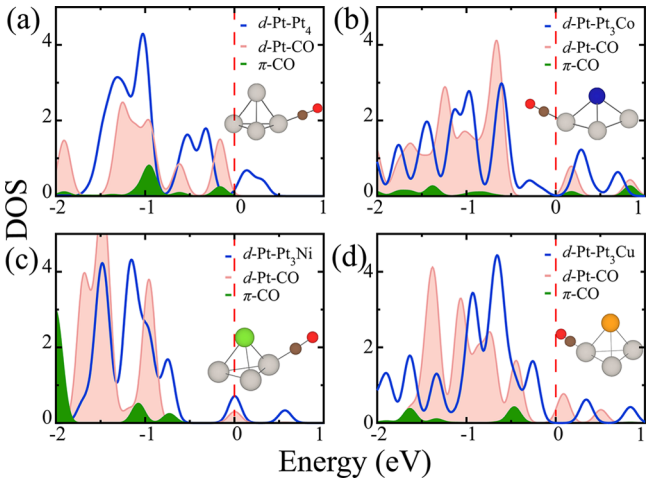

Figure 2. Partial density of states (PDOS) plot of Pt d-states without (blue) and with (pink) CO adsorbed, and the π-orbital of CO (green) for (a) Pt_4, (b) Pt_3Co, (c) Pt_3Ni, and (d) Pt_3Cu.

adsorbs on the clusters with the carbon end on mode taking a slightly tilted geometry with respect to the clusters. The C−O bond lengthens to 1.16 from 1.14 Å after adsorption because of the back-donation of electrons from the metal to the CO π-orbital. The adsorption energies of CO on Pt atom of Pt_4, Pt_3Co, Pt_3Ni, and Pt_3Cu clusters are −2.86, −3.05, −2.92, and −2.88 eV, respectively. Going from left to right of the periodic table, the adsorption energy decreases with increasing number of d-electrons of the M. This can be explained from the charge density plot (Figure 1b), where the charge depletion on Pt is maximum for Pt_3Co and least for Pt_3Cu. It is observed that CO adsorption energy on the Pt atom is higher on bimetallic free-standing clusters than on a pure Pt_4 cluster. This is expected as charge has been transferred from Pt atoms to the transition metal in the cluster, making Pt more deficient of charge and more reactive toward CO. Interestingly, CO also gets adsorbed on the Co atom with only 0.47 eV higher energy than that for Pt atom. This competitive adsorption, however, is absent for Ni and Cu atoms in their respective bimetallic clusters as the energy is ∼2 eV higher on these than on Pt. Hence, for free-standing Pt_3Co, there is a statistical possibility for CO to adsorb on the Co atom rather than on Pt. This implies that if CO adsorbs on the Co atom rather than Pt in the bimetallic cluster, the problem of Pt poisoning can be effectively solved.

In order to study the complete CO oxidation, oxygen was then adsorbed on the clusters, which already have CO adsorbed on them. Pt_4, Pt_3Co, Pt_3Ni, and Pt_3Cu clusters adsorb oxygen in the superoxo state[6] with binding energies of −1.91, −1.84, −1.85, and −1.87 eV, respectively. The oxygen adsorption energies, as observed, are complementary to CO adsorption energies. The least binding energy of oxygen is on Pt_3Co, which gave the highest binding energy for CO among the bimetallic clusters. The number of d-states filled by π-states of CO

DOI: 10.1021/cs501911r
ACS Catal. 2015, 5, 1826−1832

decreases from Co to Ni to Cu, and hence the charge transfer from the cluster to π-orbital of O_2 is more strongly facilitated in this particular order. Although the electronic structures of Pt([Xe]4f^{14}5d^{9}6s) and Ni([Ar]3d^{8}4s^2) are similar to those of Pt compared to Co([Ar]3d^{7}4s^2) and Cu([Ar]3d^{10}4s^1), the presence of Ni also increases the spin state of Pt_3Ni. Spin density and O_2 adsorption energy show a very strong correlation.[39] Therefore, Co, Ni, and Cu make Pt-based complexes more reactive due to more unpaired electrons.

To gain further insight into the mechanisms of CO and O_2 adsorption, a PDOS plot is shown in Figure 2. The adsorbed CO π-orbital overlaps most with the Pt d-state in the case of Pt_3Co (Figure 2b) as compared to Pt_4 (Figure 2a), Pt_3Ni (Figure 2c), and Pt_3Cu (Figure 2d). Pt d-states in Pt_3Co overlap with CO π-states above the Fermi level along with the states below it. This strong overlap is responsible for the small adsorption strength of O_2 on Pt_3Co than on the other clusters. The Pt_3Co cluster suffers slight deformation, as seen in Figure 2b, due to the strong adsorption of CO. Figure 2d shows that the overlap of CO π-states is the least with Pt d-states in the Pt_3Cu cluster. The available Pt d-states are more compared to the other clusters, and hence O_2 adsorbs most strongly here.

Next, we consider the kinetics of CO oxidation by molecular O_2, which has been vastly reported to proceed via the Langmuir–Hinshelwood (L–H)[40,41] mechanism. This is because the reaction barrier for the L–H mechanism is quite lower than the desorption energies of CO and O_2.[42] The free-standing clusters with CO and O_2 coadsorbed onto them are then examined for CO oxidation. The L–H mechanism of CO oxidation on the clusters is divided into two half-reactions. The first half of the reaction CO + 1/2O_2 → CO_2 involves breaking of the superoxo bond. For the second half of the reaction CO + O → CO_2, the CO oxidation barrier is dependent on the breaking of the Pt/M–O bond. Among the Pt_3M, the barriers for the L–H CO oxidation were found to be the lowest for M = Co, with the barrier being 0.36 eV (E_{b1}) and 0.42 eV (E_{b2}) for the first and second half-reactions, respectively. The full reaction pathway depicting the CO oxidation barrier on free-standing Pt_3Co is shown in Figure 3. It can be seen from Figure 3 that TS1 is the first transition state in the complete L–H mechanism of CO oxidation by molecular O_2, involving the breaking of the superoxo bond. The FS1 is the intermediate final state or the end state of the first half-reaction of CO oxidation. The oxygen atom is now activated on both the Pt and Co sites of the cluster and reacts readily with the next adsorbed CO. E_{b1} and E_{b2} values for Pt_4, Pt_3Cu, and Pt_3Ni are 0.41 and 0.49 eV, 0.39 and 0.42 eV, and 0.56 and 0.61 eV, respectively. The reaction pathways for these systems are shown schematically in Figure S2. Therefore, Pt_4, Pt_3Cu, and Pt_3Co have very similar catalytic activity in terms of kinetics. However, the possibility of no Pt poisoning along with kinetics better than that of pristine Pt_4 makes the Pt_3Co the most attractive candidate as a CO oxidation catalyst in this study.

Having shown the efficiency of free-standing clusters for CO oxidation, providing a suitable support and assessing its effects on the catalytic activity are essential. The next step was to conduct CO oxidation on clusters supported on an oxide, as this enhances catalytic activity of nanoclusters.[43,44] The choice was a simple oxide surface MgO(100) prone to vacancy formation and could be easily synthesized.[45,46] Complete relaxation of the Pt-based bimetallic clusters was done on this surface, followed by CO adsorption on each. The clusters have very strong binding energies on MgO(100), calculated as E_b = $E_{cluster/MgO(100)} - E_{MgO(100)} - E_{cluster}$, where "cluster" is Pt_4 and Pt_3M. The binding energies were −6.33, −5.65, −5.49, and −5.02 eV for Pt_3Co, Pt_3Ni, Pt_3Cu, and Pt_4, respectively. The binding energy is greatest in the case of Pt_3Co, which is expected because the highest charge redistribution was in this free-standing cluster. Interestingly, CO adsorbs with a weaker binding energy on these supported clusters compared to the free-standing clusters. The adsorption energies for CO on Pt_3Co, Pt_3Ni, Pt_3Cu, and Pt_4 on MgO(100) were calculated to be −0.9, −1.45, −1.53, and −1.92 eV, respectively. In Pt_3Ni, Pt_3Cu, and Pt_4, CO energetically prefers the Pt atoms as the adsorption site by ∼1.2 eV, whereas the favorable site on Pt_3Co is the Co atom by an energy difference of 0.8 eV.

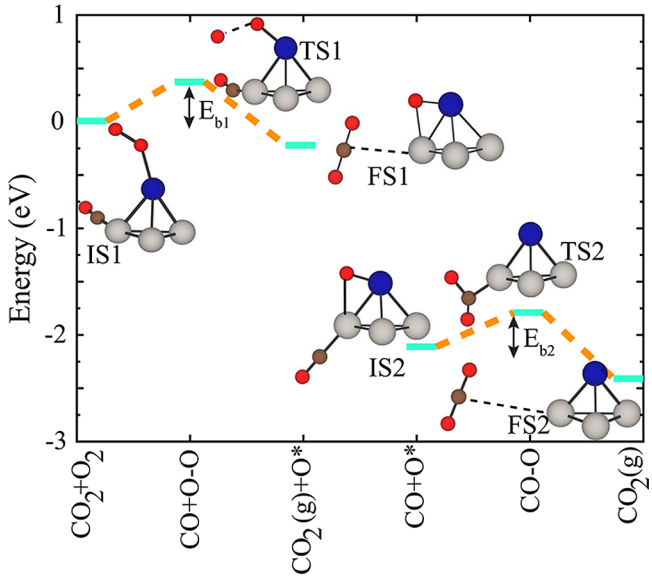

Figure 3. L–H mechanism reaction pathway and barrier for CO oxidation on free-standing Pt_3Co. L–H mechanism of CO oxidation on the clusters is divided into two half-reactions. The first half of the reaction CO + 1/2O_2 → CO_2 and the second half of the reaction CO + O → CO_2 are shown separately with 1 and 2. IS1 is the starting point of first half of the L–H mechanism of CO oxidation, referenced arbitrarily at 0. TS1 is the first transition state, and FS1 is the final step of the first half of the L–H mechanism. IS2 is the initial state of the second half-reaction. The beginning energy of IS2 is arbitrarily taken for pictorial representation. TS2 is the transition state of the second half of L–H and is referenced from IS2, giving FS2 as the final step of the complete L–H mechanism. Silver, blue, red, and brown atoms represent Pt, Co, O, and C, respectively.

The change in the catalytic properties of the clusters due to the support can be understood better by looking into the electronic structure of the systems.[47,48] The d-band model introduced by Norskov and Hammer[49] is very useful in explaining the adsorption strength of adsorbents on transition metals.[50,51] Figure 4 is the representation of the distance of the d-band center from the Fermi energy. The lower the d-band centers from the Fermi energy, the fewer empty antibonding states are available for CO adsorption.[49,50] In Figure 4, for free-standing Pt_3Co, the d-band centers of Pt and Co atoms lie very close to each other, explaining the competitive adsorption of CO on this cluster. The d-band center of Pt, however, is closer to the Fermi level than that for Co. Hence, for CO adsorption, the Pt atom is the preferred site. The d-band centers of the Pt atom in Pt_3Ni and Pt_3Cu are closer to the Fermi level than that of Ni and Cu atoms, in their respective clusters. Also, the d-band centers of Ni and Cu are far below that of Pt, eliminating

DOI: 10.1021/cs501911r
ACS Catal. 2015, 5, 1826–1832

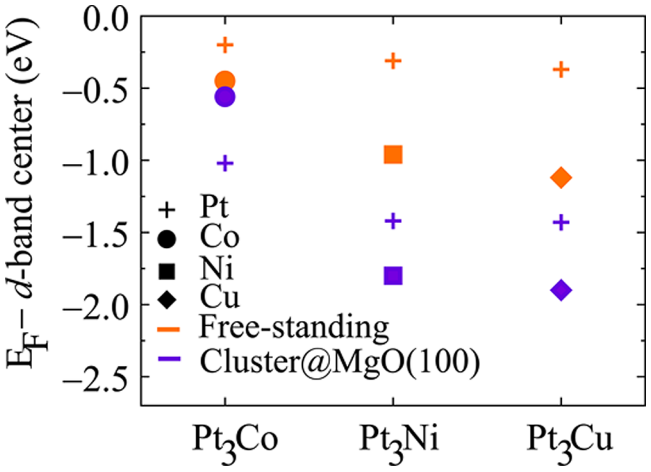

Figure 4. Center position of the d-band relative to the Fermi level for the free-standing clusters (orange) and for clusters supported on MgO(100) (blue).

the chance of competitive adsorption of CO on Pt and M sites. Hence, CO prefers only the Pt atom site in these clusters. The position of the d-band centers shown here also explains the CO adsorption strength. As the highest number of antibonding states are for the Pt atom in Pt_3Co and least for Pt in Pt_3Cu, the adsorption of CO on Pt_3Co is maximum and is the least for Pt_3Cu. In the supported case, as shown in Figure 4, for the Pt_3Co cluster, the antibonding states of Co are more available in terms of energy and number than those of the Pt atom. Pt atoms bind very strongly to MgO(100), utilizing their antibonding states that are available for CO adsorption, which causes a downshift of the Pt d-band center below than that of Co. Therefore, the CO prefers to adsorb at the Co site. On the other hand, the d-band centers of Pt in Pt_3Ni and Pt_3Cu are closer to the Fermi level than those of Ni and Cu atoms. This is due to their relative position in the free-standing cluster where the d-band centers of Ni and Cu are far below that of Pt. Therefore, CO adsorption occurs on Pt sites of these clusters. Also, as shown in Figure 4, the d-band centers of Pt are lowered in the supported clusters compared to the free-standing case, explaining the reduced adsorption energies obtained for CO in each case. Therefore, the d-band center position relative to Fermi energy is a good indicator of the favorable adsorption site in a system and can be an effective tool to design catalysts with no Pt poisoning.

To further investigate the role of electronic structure for this very interesting CO adsorption site inversion that occurs only for Pt_3Co, we calculate the PDOS of the bimetallic systems supported on MgO(100). From Figure 5, it is seen that the empty antibonding d-states of Pt in Pt_3Co overlap perfectly and completely with O p-states of MgO(100). The antibonding empty d-states are essential for CO adsorption, which are completely taken up by the oxygen of MgO(100) in the case of Pt_3Co. This is not the case in Pt_3Ni and Pt_3Cu, where the antibonding d-states of Pt atoms are still empty after complete attachment of clusters on MgO(100). Thus, the Pt site remains unaffected in Pt_3Co, and CO adsorbs on Co, whereas in the other clusters, the CO prefers to adsorb on the Pt site of the clusters.

Even though Pt_3Co emerges as our best option to avoid Pt poisoning, the reaction kinetics still need to be considered. Therefore, CO oxidation was studied only on the supported

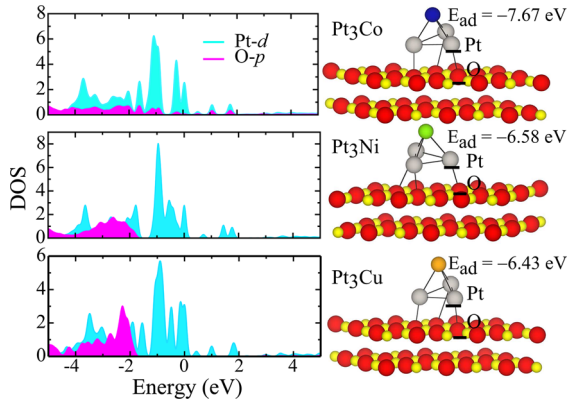

Figure 5. PDOS of Pt d-states with 2p-states of O_2 for Pt_3Co, Pt_3Ni, and Pt_3Cu. The underlined atoms depict the atoms chosen for the DOS plot. Silver, blue, green, gold, yellow, red, and brown represent Pt, Co, Ni, Cu, Mg, O, and C, respectively.

Pt_3Co cluster. Oxygen adsorbs here in the peroxo state with a binding energy of −1.63 eV, unlike the superoxo state in free-standing clusters. The adsorption of oxygen in the peroxo state at the same site of CO results in a spontaneous first half-reaction of CO oxidation of IS1 to FS1 ($CO + 1/2O_2 \rightarrow CO_2$), through TS1 with a reaction barrier as small as 0.03 eV, as shown in Figure 6. To complete the L−H mechanism of CO

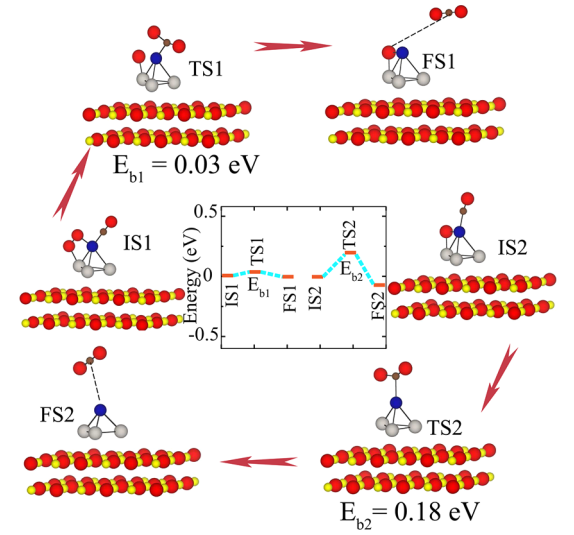

Figure 6. Minimum energy pathway and the reaction barrier for the L−H mechanism of CO oxidation on Pt_3Co supported on MgO(100). Silver, blue, green, gold, yellow, red, and brown represent Pt, Co, Ni, Cu, Mg, O, and C, respectively.

oxidation, the second half of the reaction ($CO + O \rightarrow CO_2$) requires the activated O atom in IS2 to react with another CO molecule to reach FS2. This proceeds through TS2, as shown in Figure 6, with an energy barrier of 0.18 eV.

Although, the L−H mechanism is most widely known for CO oxidation, it is intensively dependent on both oxygen and CO coverages. The variations of pressure cause a difference in adsorbate coverages, which effectively limits the CO oxidation.[52] It is, hence, essential to assess the feasibility of the MvK mechanism, as well, common on oxide surfaces, where a lattice oxygen readily interacts with the adsorbed CO on the cluster. The reaction barrier and pathway calculated for this

DOI: 10.1021/cs501911r
ACS Catal. 2015, 5, 1826−1832

case on $Pt_3Co/MgO(100)$ was ~7 eV. The high barrier is due to the large oxygen vacancy formation energy in pristine MgO(100). Doping of MgO(100) surfaces has been shown to lower the vacancy formation energy.[53−55] Previous works suggest that dopants can lower the vacancy formation energy of the host oxide and, thus, promote the oxidation reaction by the MvK mechanism.[56,57] Here, we dope the MgO(100) surface with two Li atoms to model a charge-stabilized system, which loses a lattice O. It was found that doping the substrate with Li is stable and promotes the MvK mechanism of CO oxidation on these systems. Furthermore, anchoring the cluster on Li-doped MgO(100) activates a spontaneous oxygen vacancy.

The better anchoring on Li-doped MgO(100) compared to that on MgO(100) and the spontaneous oxygen vacancy can be explained from the charge redistribution plots, shown in Figure 7, calculated as

$$\Delta\rho = \rho(Pt_4[Pt_3M/MgO])[Pt_4[Pt_3M/Li{-}MgO]]$$

$$-\rho(MgO)[Li{-}MgO] - \rho(Pt_4[Pt_3M])$$

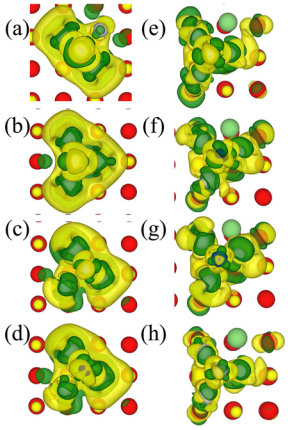

Figure 7. Charge redistribution plotted for (a) Pt_4, (b) Pt_3Co, (c) Pt_3Ni, and (d) Pt_3Cu supported on MgO(100) and (e) Pt_4, (f) Pt_3Co, (g) Pt_3Ni, and (h) Pt_3Cu supported on Li-doped MgO(100). Yellow and green represent the charge accumulation and depletion, respectively. Yellow, red, and green atoms represent Mg, O, and Li, respectively.

where $\rho(Pt_4[Pt_3M/MgO][Pt_4[Pt_3M/Li{-}MgO)]$, $\rho(MgO[Li{-}MgO])$, and $\rho(Pt_4/\ Pt_3M])$ are the charge densities of bimetallic clusters on MgO(100) or Li-doped MgO(100), isolated systems of MgO(100) or Li-doped MgO(100), and Pt_4 or Pt_3TM, respectively. Figure 7a shows that the charge redistribution in $Pt_4/MgO(100)$ is small compared to the rest of the systems. The charge redistribution is greatest in the case of Pt_3Co, and the accumulation is very symmetric, as shown in Figure 7b, around Pt atoms due to the unavailability of empty d-states, leaving Pt atoms of the cluster unavailable for CO adsorption. The charge redistribution further increases on the Li-doped MgO(100), showing better adsorption of the clusters on the substrate. In Figure 7e−h, the clusters on Li-doped MgO(100) show an interaction with lattice O through large charge redistribution around it. Therefore, when placed on Li-doped MgO(100), the interaction of the clusters with MgO(100) is to an extent to activate an oxygen vacancy spontaneously. This is in agreement with previous studies that show that the presence of dopants weakens the bonds between lattice oxygen and metal in metal oxide.[58]

The doped substrate shows better stability of Pt_3Co than pristine MgO(100) and hence gives a lower CO adsorption energy of −0.63 eV. The CO adsorption in this case also occurs preferably on the Co site itself. The potential energy profile indicating the energetically most preferable site for CO attachment is depicted in Figure S3. The charge redistribution in Figure 7 also shows that it is the cluster that causes an excess interaction with the oxygen atom between the two Li atoms, causing it to come out of the lattice. The MvK reaction barrier on the Pt_3Co/Li-doped MgO(100) was calculated to be 0.11 eV. Figure 8 depicts the reaction pathway and barrier of 0.11 eV

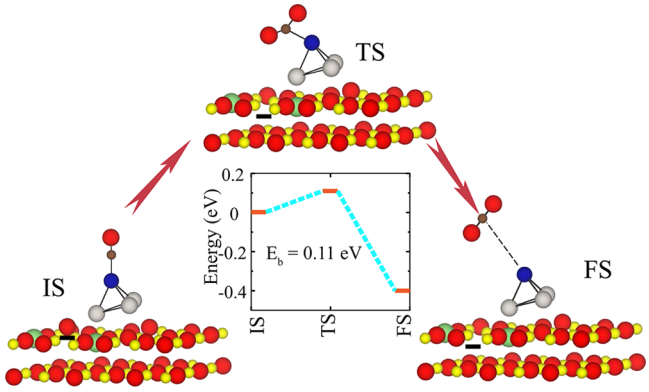

Figure 8. Minimum energy pathway and the reaction barrier for the MvK mechanism of CO oxidation on Pt_3Co supported on Li-doped MgO(100). Silver, blue, green, yellow, red, and brown represent Pt, Co, Li, Mg, O, and C, respectively.

for the most efficient system of Pt_3Co on Li-doped MgO. The reaction proceeds through a TS of capturing the O atom by CO. The vacancy formation energy needed is almost barrierless. To further depict the reaction path of lattice O combining with CO on the Co site, we scan the potential energy surface in the vicinity of the area of the reaction. The reaction path is shown in Figure S4, where we get a similar barrier of 0.10 eV for capturing the lattice O by CO to form CO_2. Therefore, Pt_3Co on Li-doped MgO prohibits Pt poisoning by CO and also gives fast reaction kinetics via the MvK mechanism.

CONCLUSION

We studied the free-standing and MgO(100)-supported Pt_4 and Pt_3M (where M = Co, Ni, and Cu) as CO oxidation catalysts. The presence of competitive adsorption sites of Co and Pt differing by 0.47 eV in free-standing Pt_3Co opened a possibility for solving the critical problem of Pt degradation by CO. The low L−H reaction barrier obtained for CO oxidation on a Pt_3Co free-standing cluster compared to that on pristine Pt_4 also shows good reaction kinetics. Using MgO(100) as a support for clusters, it was found that MgO(100) provides good anchoring of the clusters and lowers the poisoning due to CO on each cluster due to the lowering of the d-band centers. There is a one-to-one correspondence of the d-band center and the CO adsorption strength. Also, the relative position of d-band centers from the Fermi level efficiently indicates the favorable adsorption site in a system. Most remarkably, Pt_3Co/MgO(100) has Co as the preferable site for CO adsorption rather than Pt, solving the critical problem of Pt poisoning. MgO(100) further brought down the L−H reaction barrier of CO oxidation on Pt_3Co to a lower value. CO oxidation through

DOI: 10.1021/cs501911r
ACS Catal. 2015, 5, 1826−1832

lattice oxygen on pure MgO(100) was very difficult as the oxygen vacancy formation energy is more than 7 eV. The vacancy formation became spontaneous when Pt_3Co was anchored on Li-doped MgO(100). The clusters interacted through a large charge transfer with lattice oxygen and activated a spontaneous oxygen vacancy. Hence, MvK on Li-doped MgO(100) gave lower reaction barrier of 0.11 eV on the most efficient Pt_3Co cluster. The conclusions drawn from this work can be extended to design efficient catalysts for other important reactions such as ORR, hydrogenation, and water splitting.

■ ASSOCIATED CONTENT

Supporting Information

The following file is available free of charge on the ACS Publications website at DOI: 10.1021/cs501911r.

Details of the tetrahedral geometry of pristine Pt_4, L-H mechanism reaction pathway on Pt_4, Pt_3Ni, and Pt_3Cu, and potential energy surface scanning of the CO adsorption and the MvK mechanism of CO oxidation by lattice oxygen on Pt_3Co/Li-doped MgO(100) (PDF)

■ AUTHOR INFORMATION

Corresponding Author

*E-mail: abhishek@mrc.iisc.ernet.in.

Notes

The authors declare no competing financial interest.

■ ACKNOWLEDGMENTS

This work was financially supported by DST Nanomission. The authors thank Materials Research Center, Indian Institute of Science, Bangalore, for providing the required computational facilities. R.A. acknowledges support from DST through the INSPIRE Fellowship. The authors are also grateful to Prof. N. Ravishankar for his valuable discussions.

■ REFERENCES

(1) Igarashi, H.; Uchida, H.; Suzuki, M.; Sasaki, Y.; Watanabe, M. *Appl. Catal. A: Gen.* **1997**, *159*, 159−169.
(2) Potter, N. M. *Anal. Chem.* **1976**, *48*, 531−534.
(3) Li, X.-N.; Yuan, Z.; He, S.-G. *J. Am. Chem. Soc.* **2014**, *136*, 3617−3623.
(4) Liu, C.; Tan, Y.; Lin, S.; Li, H.; Wu, X.; Li, L.; Pei, Y.; Zeng, X. C. *J. Am. Chem. Soc.* **2013**, *135*, 2583−2595.
(5) Guzman, J.; Carrettin, S.; Corma, A. *J. Am. Chem. Soc.* **2005**, *127*, 3286−3287.
(6) Yamazoe, S.; Koyasu, K.; Tsukuda, T. *Acc. Chem. Res.* **2014**, *47*, 816−824.
(7) Bonanni, S.; Ait-Mansour, K.; Harbich, W.; Brune, H. *J. Am. Chem. Soc.* **2014**, *136*, 8702−8707.
(8) Ebrahimi, M.; Simonovis, J. P.; Zaera, F. *J. Phys. Chem. Lett.* **2014**, *5*, 2121−2125.
(9) Sneed, B. T.; Young, A. P.; Jalalpoor, D.; Golden, M. C.; Mao, S.; Jiang, Y.; Wang, Y.; Tsung, C.-K. *ACS Nano* **2014**, *8*, 7239−7250.
(10) Yamamoto, H.; Miyajima, K.; Yasuike, T.; Mafune, F. *J. Phys. Chemistry A* **2013**, *117*, 12175−12183.
(11) Lang, S. M.; Fleischer, I.; Bernhardt, T. M.; Barnett, R. N.; Landman, U. *J. Phys. Chem. A* **2014**, *118*, 8572−8582.
(12) Shan, S.; Petkov, V.; Yang, L.; Luo, J.; Joseph, P.; Mayzel, D.; Prasai, B.; Wang, L.; Engelhard, M.; Zhong, C.-J. *J. Am. Chem. Soc.* **2014**, *136*, 7140−7151.
(13) Norskov, J. K.; Rossmeisl, J.; Logadottir, A.; Lindqvist, L.; Kitchin, J. R.; Bligaard, T.; Jonsson, H. *J. Phys. Chem. B* **2004**, *108*, 17886−17892.
(14) Takahashi, M.; Imaoka, T.; Hongo, Y.; Yamamoto, K. *Angew. Chem., Int. Ed.* **2013**, *52*, 7419−7421.
(15) Iyyamperumal, R.; Zhang, L.; Henkelman, G.; Crooks, R. M. *J. Am. Chem. Soc.* **2013**, *135*, 5521−5524.
(16) Hwang, S. J.; Kim, S.-K.; Lee, J.-G.; Lee, S.-C.; Jang, J. H.; Kim, P.; Lim, T.-H.; Sung, Y.-E.; Yoo, S. J. *J. Am. Chem. Soc.* **2012**, *134*, 19508−19511.
(17) Cai, Q.; Wang, X.; Wang, J.-G. *J. Phys. Chem. C* **2013**, *117*, 21331−21336.
(18) Cordonna, G. W.; Kosanovich, M.; Becker, E. R. *Platinum Metals Rev.* **1989**, *33*, 46−54.
(19) Shi, Y.; Ervin, K. M. *J. Chem. Phys.* **1998**, *108*, 1757−1760.
(20) Park, J. B.; Ratliff, J. S.; Ma, S.; Chen, D. A. *J. Phys. Chem. C* **2007**, *111*, 2165−2176.
(21) Yancey, D. F.; Zhang, L.; Crooks, R. M.; Henkelman, G. *Chem. Sci.* **2012**, *3*, 1033−1040.
(22) Lang, H.; Maldonado, S.; Stevenson, K. J.; Chandler, B. D. *J. Am. Chem. Soc.* **2004**, *126*, 12949−12956.
(23) Ahmadi, M.; Behafarid, F.; Cui, C.; Strasser, P.; Cuenya, B. R. *ACS Nano* **2013**, *7*, 9195−9204.
(24) Dupont, C.; Jugnet, Y.; Loffreda, D. *J. Am. Chem. Soc.* **2006**, *128*, 9129−9136.
(25) Song, C.; Ge, Q.; Wang, L. *J. Phys. Chem. B* **2005**, *109*, 22341−22350.
(26) Kitchin, J. R.; Norskov, J. K.; Barteau, M. A.; Chen, J. G. *J. Chem. Phys.* **2004**, *120*, 10240−10246.
(27) Christoffersen, E.; Liu, P.; Ruban, A.; Skriver, H.; Norskov, J. *J. Catal.* **2001**, *199*, 123−131.
(28) Fernandez, J. L.; Walsh, D. A.; Bard, A. J. *J. Am. Chem. Soc.* **2005**, *127*, 357−365.
(29) Komatsu, T.; Tamura, A. *J. Catal.* **2008**, *258*, 306−314.
(30) Sheppard, D.; Terrell, R.; Henkelman, G. *J. Chem. Phys.* **2008**, *128*, 134106.
(31) Henkelman, G.; Arnaldsson, A.; Jonsson, H. *J. Chem. Phys.* **2006**, *124*, 044706.
(32) Lei, X. L.; Wu, M. S.; Liu, G.; Xu, B.; Ouyang, C. Y. *J. Phys. Chem. A* **2013**, *117*, 8293−8297.
(33) Shi, Y.; Ervin, K. *J. Chem. Phys.* **1998**, *108*, 1757−1760.
(34) Heiz, U.; Sanchez, A.; Abbet, S.; Schneider, W. D. *J. Am. Chem. Soc.* **1999**, *121*, 3214−3217.
(35) Kyuno, K.; Ehrlich, G. *Surf. Sci.* **1999**, *437*, 29−37.
(36) Zhou, M.; Zhang, A.; Dai, Z.; Zhang, C.; Feng, Y. P. *J. Chem. Phys.* **2010**, *132*, 194704.
(37) Henkelman, G.; Arnaldsson, A.; Jonsson, H. *Comput. Mater. Sci.* **2006**, *36*, 354−360.
(38) Sanville, E.; Kenny, S. D.; Smith, R.; Henkelman, G. *J. Comput. Chem.* **2007**, *28*, 899−908.
(39) Kobayashi, H.; Tomoya, N.; Miyazaki, S.; Miura, T.; Takeuchi, N.; Yamabe, T. *Mater. Sci. Eng.* **2011**, *18*, 122010.
(40) Moseler, M.; Walter, M.; Yoon, B.; Landman, U.; Habibpour, V.; Harding, C.; Kunz, S.; Heiz, U. *J. Am. Chem. Soc.* **2012**, *134*, 7690−7699.
(41) Kunz, S.; Schweinberger, F. F.; Habibpour, V.; Rottgen, M.; Harding, C.; Arenz, M.; Heiz, U. *J. Phys. Chem. C* **2010**, *114*, 1651−1654.
(42) Baxter, R. J.; Hu, P. *J. Chem. Phys.* **2002**, *116*, 4379−4381.
(43) Harding, C.; Habibpour, V.; Kunz, S.; Farnbacher, A. N.-S.; Heiz, U.; Yoon, B.; Landman, U. *J. Am. Chem. Soc.* **2009**, *131*, 538−548.
(44) Yoon, B.; Hakkinen, H.; Landman, U.; Wrz, A. S.; Antonietti, J.-M.; Abbet, S.; Judai, K.; Heiz, U. *Science* **2005**, *307*, 403−407.
(45) Uberuaga, B. P.; Smith, R.; Cleave, A. R.; Henkelman, G.; Grimes, R. W.; Voter, A. F.; Sickafus, K. E. *Phys. Rev. B* **2005**, *71*, 104102.
(46) Henkelman, G.; Uberuaga, B. P.; Harris, D. J.; Harding, J. H.; Allan, N. L. *Phys. Rev. B* **2005**, *72*, 115437.
(47) Tang, W.; Henkelman, G. *J. Chem. Phys.* **2009**, *130*, 194504.
(48) Lu, C. Y.; Henkelman, G. *J. Phys. Chem. Lett.* **2011**, *2*, 1237−1240.

DOI: 10.1021/cs501911r
ACS Catal. 2015, 5, 1826−1832

(49) Hammer, B.; Norskov, J. K. *Nature* **2002**, *376*, 238−240.
(50) Tang, W.; Zhang, L.; Henkelman, G. *J. Phys. Chem. Lett.* **2011**, *2*, 1328−1331.
(51) Zhou, W.-P.; Yang, X.; Vukmirovic, M. B.; Koel, B. E.; Jiao, J.; Peng, G.; Mavrikakis, M.; Adzic, R. R. *J. Am. Chem. Soc.* **2009**, *131*, 12755−12762.
(52) Bobaru, S. High-Pressure STM Studies of Oxidation Catalysis. Ph.D. Thesis Leiden University, 2006.
(53) Prada, S.; Giordano, L.; Pacchioni, G. *J. Phys. Chem. C* **2012**, *116*, 5781−5786.
(54) Pacchioni, G.; Pescarmona, P. *Surf. Sci.* **1998**, *412413*, 657−671.
(55) Kim, H. Y.; Henkelman, G. *J. Phys. Chem. Lett.* **2012**, *3*, 2194−2199.
(56) Kim, H. Y.; Lee, H. M.; Pala, R. G. S.; Shapovalov, V.; Metiu, H. *J. Phys. Chem. C* **2008**, *112*, 12398−12408.
(57) Bonanni, S.; Ait-Mansour, K.; Harbich, W.; Brune, H. *J. Am. Chem. Soc.* **2012**, *134*, 3445−3450.
(58) Kim, H. Y.; Lee, H. M.; Henkelman, G. *J. Am. Chem. Soc.* **2012**, *134*, 1560−1570.

DOI: 10.1021/cs501911r
ACS Catal. 2015, 5, 1826−1832